RSC Advances

PAPER

View Article Online
View Journal | View Issue

Cite this: *RSC Adv.*, 2024, **14**, 15953

Effects of crack–γ/γ' interface relative distributions on the deformation and crack growth behaviors of a nickel-based superalloy

Xinmao Qin, [abcd] Wanjun Yan, [b] Yilong Liang*[acd] and Fei Li[acd]

Using the molecular dynamics (MD) method, we investigated the effects of crack distributions on the deformation and crack growth of a nickel (Ni)-based superalloy. The results indicated that as the distance between two cracks increased, both tensile strength and plasticity decreased, while the crack growth rate significantly increased. In systems with short crack distances, strong interactions occurred between the dislocations that emitted from two cracks and the γ/γ' interface mismatched dislocation network. These interactions led to an overlap in the plastic zones ahead of the crack tips at the γ/γ' interface, which resulted in significant passivation at the front and middle regions of the cracks. Consequently, the two cracks merged in the *X*-direction to form a wide crack. The cracks coalescence consumed a lot of external deformation work, resulting in the highest tensile strength and plasticity. In this study, we proposed a potential approach to simultaneously enhance the strength and plasticity of multidefect systems, providing a theoretical basis for explaining deformation mechanisms and crack growth in these systems.

Received 11th April 2024
Accepted 12th May 2024

DOI: 10.1039/d4ra02723j

rsc.li/rsc-advances

1. Introduction

Nickel-based superalloys, a type of aging strengthened alloy widely used at present, contain numerous coherent precipitates, such as the γ' (Ni_3Al) and γ'' (Ni_3Nb) phases. These precipitates significantly enhance the strength of the alloy at room and elevated temperature. Because of their excellent properties, such as corrosion resistance and high strength, these superalloys are commonly used in components, for example, oil slinger drum shafts and turbine disk connection bolts for aircraft engines, as well as wind power connection bolts, and key components for marine engineering.[1–3] The plastic deformation and fracture failure of mechanical components occur primarily during service. The fracture of a mechanical component consists of crack initiation and crack growth at the macroscopic level. The microscopic mechanism of fracture refers to the chemical bond constantly broken between atoms, which determines the crack initiation and growth process of mechanical components on a macroscopic scale, and ultimately determines their mechanical properties. The mechanical components inevitably contain microscopic voids, cracks, and other defects, which alter the microstructure evolution during deformation and the corresponding mechanical properties. Therefore, it is necessary to study the effects of internal microscopic defects, such as micro-cracks, micro-voids, and grain boundaries, on the deformation and fracture. However, it is difficult to experimentally study the microstructure evolution of the deformation system in real time. The atomic-scale molecular dynamics (MD) simulation provides a feasible way for the investigation of deformation and fracture of materials. The MD method treat atoms as classical particles whose motion follows Newton's equations of motion. And the Newton's equation of motion was solved by integral algorithm to obtain the evolution of atomic position and velocity with time. So, the corresponding relationship between the microstructure of the system and its physical and mechanical properties was obtained. During deformation, the MD simulation can be used to record the atomic motion trajectory of the system in real time and to further analyze the microstructure evolution through corresponding visualization software.

To date, MD methods have been widely used to study the deformation and fracture of pure metals, including Ni,[4–11] Cu,[12,13] Al,[14–17] Ag,[18] Fe,[19–22] Mg,[23] and Ti.[24,25] In addition to pure metals, the deformation and fracture of binary nickel/nickel aluminide (Ni/Ni_3Al) alloy have been investigated using the MD method. Yashiro[26] *et al.* studied the dislocation behavior of the tip and edge of the rectangular precipitate (Ni_3Al) in the Ni matrix. Zhu,[27] Wu,[28] Li[29] and Yang[30] further investigated stability mechanism of mismatched dislocation networks at different γ (Ni)/γ' (Ni_3Al) interfaces of Ni-based superalloys. Li[31] and Chen[32] discussed the deformation behaviors and microstructure evolution of the γ/γ'

[a]*College of Materials and Metallurgy, Guizhou University, Guiyang 550025, China. E-mail: ylliang@gzu.edu.cn*

[b]*School of Electronic and Information Engineering, Anshun University, Anshun 561000, China*

[c]*Guizhou Key Laboratory for Mechanical Behavior and Microstructure of Materials, Guiyang 550025, China*

[d]*National & Local Joint Engineering Laboratory for High-Performance Metal Structure Material and Advanced Manufacturing Technology, Guiyang 550025, China*

system under shock loading. Kohler[33] *et al.* performed MD simulation of the interaction between edge dislocation of the Ni matrix phase and spherical precipitate. It was found that the interaction between dislocation and precipitate was related to the size of precipitate. Cui[34] *et al.* explored the effect of microscopic defects on the interaction between dislocation and Ni_3Al precipitate. Liu,[35] Ma,[36] Yu,[37] and Ben[38] studied the crack growth behavior of the γ/γ' system and found that the defects (*e.g.*, vacancy, dislocation), γ/γ' interface, and grain boundary had a significant impact on the crack growth. The effects of different stress states, crack locations, and orientations on fatigue crack growth in Ni-based superalloys were studied in our previous work.[39] The influence of relative distributions of multiple microscopic defect (holes or cracks) on the deformation and fracture of γ/γ' alloy is rarely studied.

In this study, we used the MD method to systematically examine the influence of the two cracks distributions relative to the γ/γ' interface on the deformation and crack growth behavior of the deformation system. The different distributions of two cracks relative to the γ/γ' interface mainly refers to the difference of the distance between the two cracks (which distributed at the two side of the γ/γ' interface) in the width (*X*-direction in our simulation model) and length (*Y*-direction in our simulation model) direction. So, we primarily investigate the distance between the two cracks in the width (*X*-direction in our simulation model) and length (*Y*-direction in our simulation model) direction on the deformation and crack propagation behavior of the Ni/Ni_3Al superalloy. By calculated the tensile strength, accumulated plastic strain, and the relationship between the crack length and strain of the deformation system with different cracks distributions, the deformation and crack propagation behavior of the Ni/Ni_3Al superalloy with different distributions of two cracks relative to the γ/γ' interface were analyzed. And further provided the microscopic mechanism of the deformation and crack growth of the system in terms of the microstructure evolution characterization of the system and fracture mechanics theory analysis. Our research provides a potential way to improve the strength and plasticity of multidefect systems (*e.g.*, internal nanopore, cracks) at the same time and provides a theoretical basis for explaining the deformation mechanism and crack growth of multidefect systems.

2. Simulation method and details

2.1 Simulation method and model

In this work, we used the Large-Scale Atomic/Molecular Massively Parallel Simulator (LAMMPS)[40] software to investigate the deformation and crack growth behaviors in Ni-based superalloy. The simulation model was composed of the γ phase (Ni) and γ' phase (Ni_3Al), as shown in Fig. 1. The dimensions of the model were 514, 257, and 257 Å for the *X* ([100]), *Y* ([010]), and *Z* ([001]) direction, respectively. To relax the mismatched stress that originated from the lattice mismatch of the γ phase and γ' phase, we selected the size of two phases of the model as $na_\gamma \approx ma_{\gamma'}$ (the *n* and *m* are positive integer numbers; $a_\gamma = 3.524$ Å and $a_{\gamma'} = 3.573$ Å). By remove some atoms of the corresponding regions in the system, we created a model with two cracks for specified distributions. It should be noted that the initial crack shape is rectangular, and its length and width is $15a_\gamma$ and $3a_\gamma$ ($a_\gamma = 3.524$ Å), respectively. At present, the deformation system with rectangular crack has been extensively applied to study the deformation and crack propagation behavior of the metals.[5,8,18,38,41,42] In this simulation, the different distributions of two cracks relative to the γ/γ' interface mainly refers to the difference of the distance between the two cracks (which distributed at the two side of the γ/γ' interface) in the width (*X*-direction in our simulation model) and length (*Y*-direction in our simulation model) direction. Therefore, we divided the model with various cracks distributions (relative to the γ/γ' phase interface) into two cases: (1) two cracks were distributed symmetrically relative to the interface, and the distance between crack1 and crack2 (d_x) in the *X*-direction was 20, 40, 60, 80, 120, 160, 200, and 240 Å (as shown in Fig. 1(b)); and (2) two cracks were distributed asymmetrically relative to the interface, and the distance d_y in the *Y*-direction was 0, 30, 60, 90, and 120 Å (as shown in Fig. 1(c)).

We applied the three-dimensional periodic boundary conditions to the simulation. Before loading, using an isothermal–isobaric ensemble (NPT), the simulation system relaxed 10 ps at a temperature of 300 K and a pressure of 0 bar. Then we performed the uniaxial tensile loading along the *X*-direction, and we used the microcanonical ensemble (NVE) in this loading stage (strain rate $\dot{\varepsilon} = 1 \times 10^9\ s^{-1}$, it should be noted that this strain rate is commonly used in molecular dynamics simulations investigation of deformation and fracture of metal systems). To verify the repeatability of the calculation results, we conducted three calculations for each model. The results showed that the calculation data obtained by the same model with different random number parameters were fundamentally consistent, which indicated that our calculation results were reliable.

2.2 The atomic interactions potential

In this work, the Ni–Ni and Ni–Al atomic interactions of the deformation system was described by eam/alloy potential,[43] which was extensively used to simulate mechanical properties of Ni/Ni_3Al superalloy. And these results shows that the eam/alloy potential can be described successfully the relationship between the microstructure evolution and mechanical properties of Ni/Ni_3Al superalloy with crack.[32,38,44] The eam/alloy potential consists of the terms:

$$E_i = F_\alpha\left(\sum_{j\neq i}\rho_\beta(r_{ij})\right) + \frac{1}{2}\cdot\sum_{j\neq i}\varnothing_{\alpha\beta}(r_{ij}) \quad (1)$$

where E_i is the total energy of the deformation system, F_α is the embedding energy which is a function of the atomic electron density $\rho_\beta(r_{ij})$, $\varnothing_{\alpha\beta}(r_{ij})$ is a pair potential interaction, α and β are the element types of atoms *i* and *j*.

2.3 The analysis method of the microstructure

To characterize the deformation and crack growth behaviors of these systems, we analyzed the evolution of microstructure and dislocations of the model using common neighbor analysis

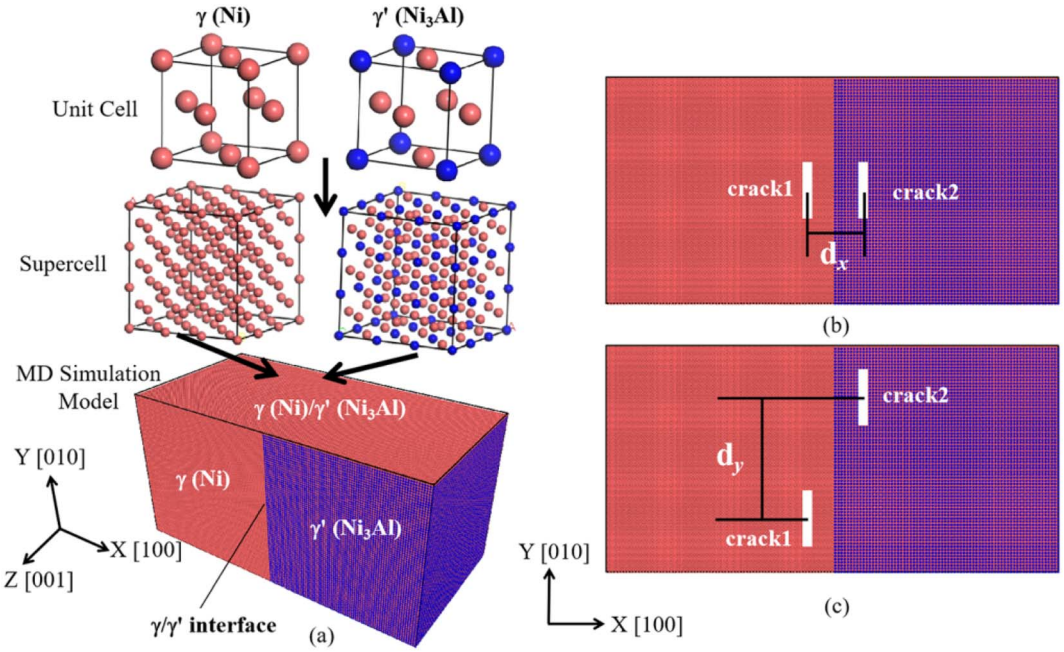

Fig. 1 The MD simulation tensile model, (a) the structure of the (Ni)/(Ni_3Al) alloy, (b) the loading condition I, (c) the loading condition II.

(CNA)[45,46] and the dislocation extraction algorithm (DXA) of the Open Visualization Tool (OVITO)[47,48] software.

3. Results

3.1 Deformation behaviors

3.1.1 Effect of crack distance (d_x) in the *X*-direction. Fig. 2(a) shows the stress–strain relationship and the tensile strength of the model with various distances between crack1 and crack2 in the *X*-direction. In the elastic deformation stage, the crack distance of the system did not have an influence on the elastic modulus. When the deformation entered the plastic stage, however, the stress–strain response of these models was noticeably different, especially for the models with the distance $d_x = 40$ Å and $d_x = 240$ Å. As the distance between crack1 and crack2 increased, the tensile strength and fracture strain of the model first increased to a maximum and then decreased. For example, the tensile strength of the model with crack distances of 20, 40, 60, 80, 120, 160, 200, and 240 Å was 9.0, 9.3, 9.1, 8.60, 8.65, 8.73, 8.16, and 8.10 GPa, respectively, and the fracture strain of the model with various crack distances was 0.34, 0.38, 0.22, 0.16, 0.10, 0.09, 0.09, 0.09, and 0.08, respectively.

Based on the stress–strain curve, we further calculated the accumulated plastic strain of the deformation system, as shown in Fig. 2(c). The accumulated plastic strain of the deformation system, which was defined as the total tensile strain at the fracture subtracting the elastic strain of the deformation system. As the distance between crack1 and crack2 increased

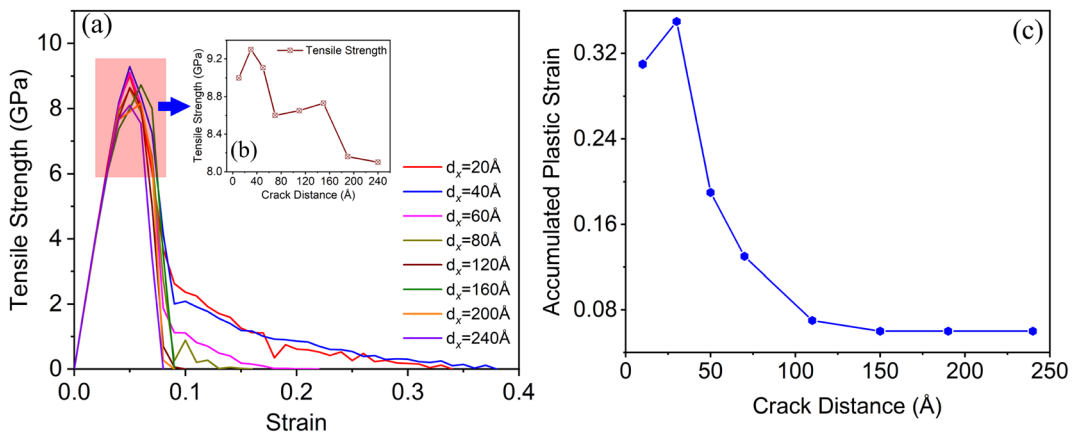

Fig. 2 Stress–strain behaviors of tensile model with various distances between crack1 and crack2 in the *X*-direction: (a) stress–strain curve, and the inset (b) denote the tensile strength of different model, and (c) accumulated plastic strain of tensile model.

from 20 to 240 Å, the accumulated plastic strain of the tensile system decreased. When the distance increased to 120 Å, the accumulated plastic strain of the tensile system remained almost unchanged. From these results, we found that the distance between crack1 and crack2 in the *X*-direction obviously affected the deformation behaviors of tensile system.

3.1.2 Effect of crack distance (d_y) in the *Y*-direction. Fig. 3 shows the stress–strain relationship, the tensile strength, and accumulated plastic strain of the tensile model with various distances between crack1 and crack2 in the *Y*-direction. We found that when the distance (d_y) changed, the deformation behavior of the system changed significantly. When $d_y = 0$ Å, the tensile strength and accumulated plastic strain of the deformation system was 9.3 GPa and 0.33, respectively. However, when $d_y = 90$ Å, the tensile strength and accumulated plastic strain decreased to 7.3 GPa and 0.06, respectively. Both the strength and plasticity of deformation system drastically deteriorated as the d_y increased.

Based on these results, as the distance between crack1 and crack2 increased, both the tensile strength and plasticity of the tensile system notably weakened. This indicated that the strength and plasticity of the multicrack system could be improved simultaneously by reducing the distance between cracks in the system.

3.2 Crack growth behaviors

Fig. 4 shows the crack length *versus* strain relationship of the tensile model with various distances between two cracks. The crack growth in the tensile process had three typical stages—namely, the crack growth incubation stage (I), the crack growth rapid stage (II), and the crack growth stable stage (III). As d_x increased from 20 Å to 240 Å, the strain consumed in the crack growth decreased, and the crack growth rate increased significantly. When d_x = 20 Å, the crack growth mainly occurred during the crack growth stable stage (III), which consumed about 30% total tensile strain, whereas the crack growth stages I and II consumed 7 and 3% total strain, respectively. When d_x increased to 60 Å, the strain consumed by the crack growth stable stage (III) accounted for about 10%, and the strain consumed in the crack growth incubation stage (I) and the rapid

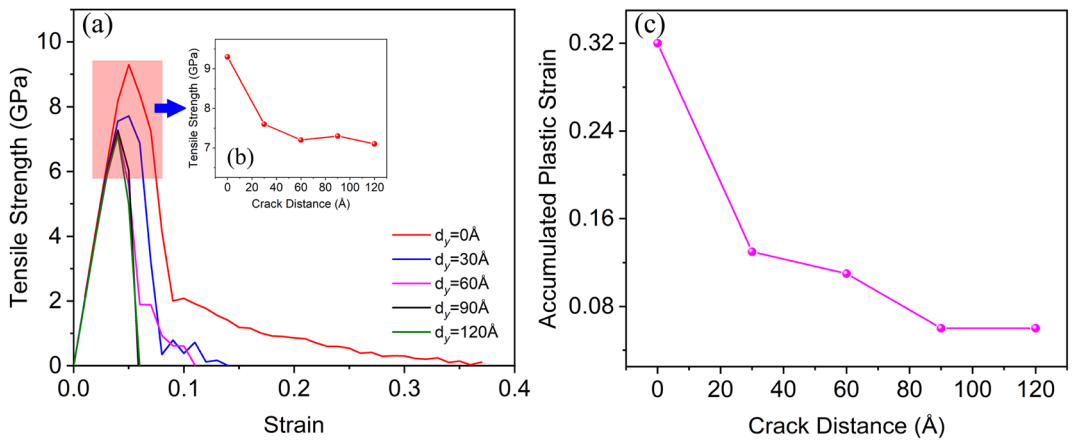

Fig. 3 Stress–strain behaviors of tensile model with various distances between two cracks in the *Y*-direction: (a) stress–strain curve, and the inset (b) denote the tensile strength of different model, and (c) accumulated plastic strain of tensile model.

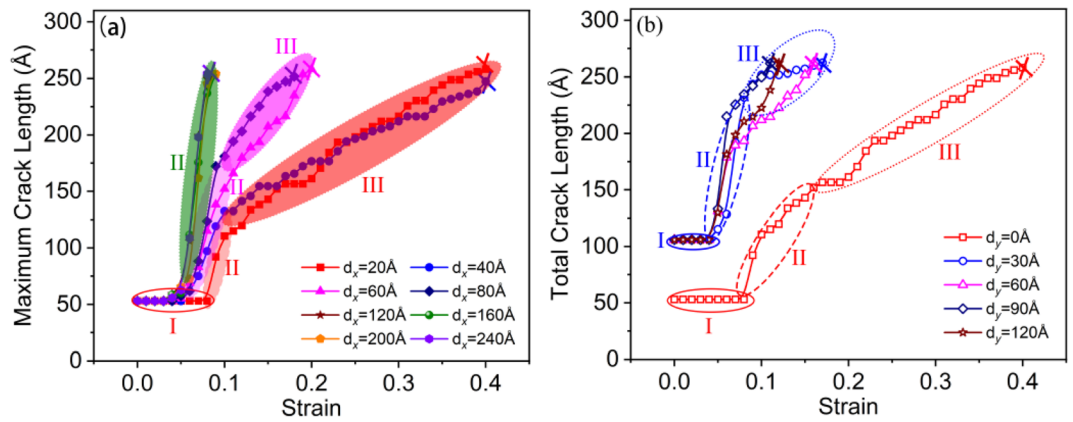

Fig. 4 Crack length *versus* strain curve of the tensile model with various distances between two cracks, (a) and (b), in the *X*- and *Y*-directions, respectively. With the change of d_x, the maximum crack length determined the deformation behavior, so we examined maximum crack length *versus* strain relationship, as shown in (a). However, the total crack length determined the deformation behavior of the system with different d_y, and therefore, we considered total crack length *versus* strain relationship, as shown in (b).

growth stage (II) was 5%. When d_x = 120 Å, the system completely broke at the end of stage (II) of crack growth, and there was no stable crack growth stage. For the system (d_x = 40 Å) with different d_y, as crack distance increased, the crack growth rate increased, and the plastic work consumed in the crack growth process decreased. When d_y > 30 Å, crack1 and crack2 began to propagate when the tensile strain of the system was 5%. Compared to the system when d_y = 0 Å, the crack growth rate in stage (II) obviously increased. These results showed that the distance between two cracks on both sides of the γ/γ′ interface had a significant effect on crack growth.

4. Discussion

4.1 Microstructure evolution

Fig. 5 shows the microstructure evolution Fig. 5(a1)–(h1) and dislocation configuration Fig. 5(a2)–(h2) of the system, which two cracks are distributed symmetrically relative to the interface and d_x = 40 Å. Note that the green, red, and gray atoms represent face-centered cubic, hexagonal closest packed, and amorphous structure atoms in this figure, respectively. The area represented by the red atoms is the stacking fault during the deformation process. During the relaxation of the system before deformation, a quadrilateral mismatched dislocation network consisting of four $\vec{b} = 1/2\langle 110\rangle$ dislocations formed at the γ/γ′ phase (as shown in Fig. 5(a2)), which was consistent with the results of Wu[27–29] *et al.* Because of the symmetric distribution of crack1 and crack2 relative to the γ/γ′ interface and their small distance from the interface in the deformation system, the dislocations that emitted from two cracks interacted with the mismatched dislocation network at the γ/γ′ interface (Fig. 5(b2)). When the tensile strain was 5%, the interaction between the dislocations that emitted from two cracks and the γ/γ′ interface mismatched dislocation was more pronounced. As shown in Fig. 5(c2), the γ/γ′ interface mismatched dislocation network almost completely disappeared, mainly because the mismatched dislocation ($\vec{b} = 1/2\langle 110\rangle$) first decomposed into two Shockley partial dislocations ($\vec{b} = 1/6\langle 112\rangle$) and then interacted with the dislocations emitted from two cracks. As the strain increased to 8%, a high-density dislocation concentration zone appeared at the vicinity of the crack as a result of the strong interaction of the dislocations between the two cracks. At the same time, the crystal structure of the area between the two cracks was significantly blunted (Fig. 5(e1) and (f1)), causing the two cracks to propagate in the *X*-direction and merge into a broad crack. Then, as the loading continued, the merged wide crack slowly propagated until the deformation system completely fractured. During the growth process of cracks along the *X*-direction (similar secondary crack formation and growth), a large amount of plastic deformation work was consumed, which resulted in the system having the highest tensile strength and the best plasticity, whereas cracks slowly propagated in a typical plastic manner.

For the deformation system when d_x = 60 Å (Fig. 6), the interaction between the crack emitting dislocations and the γ/γ′ interface mismatched dislocation network also occurred at the beginning of deformation. Compared with the system when d_x = 40 Å, however, the number of dislocations emitted from crack2 was relatively small, and the interaction between crack2 and the

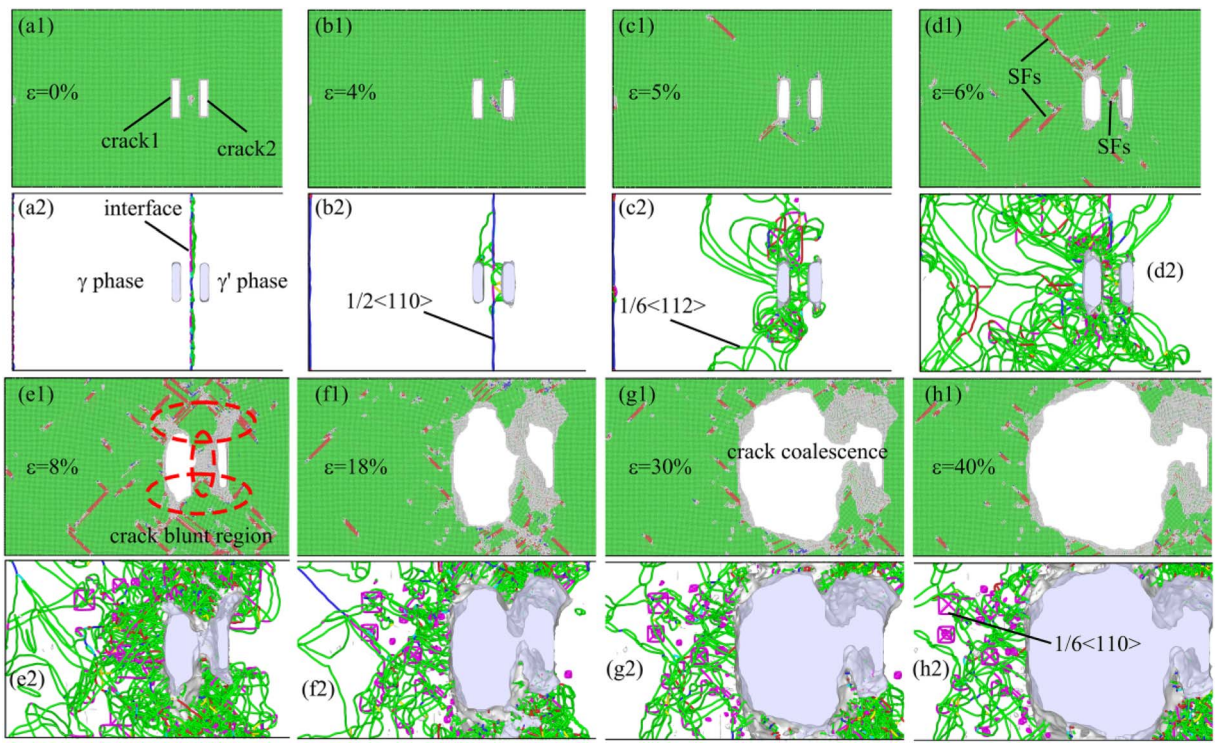

Fig. 5 The evolution of microstructure and dislocation of the tensile model when d_x = 40 Å, (a1–h1) the microstructure evolution of the tensile system at different tensile strain, (a2–h2) the dislocation configuration evolution of the tensile system at different tensile strain.

γ/γ′ interface mismatched dislocation network was relatively weak. Because the motion and interaction of dislocations that emitted from crack1 played a major role in the deformation, most of the external plastic deformation work was used for crack1 growth along the *Y*-direction. Ultimately, the tensile strength and plasticity of the system were lower than those of the system when $d_x = 40$ Å, and the crack growth rate was higher.

When the distance between two cracks in the system was $d_x = 240$ Å (Fig. 7), the crack tip first emitted dislocations during the deformation. Because of the excellent plastic deformation ability of the γ phase, the number of emission dislocations for crack1 was large, whereas the number of emission dislocations for crack2 was small. When the strain was 5%, the dislocation emitted from crack1 interacted with the γ/γ′ interface mismatched dislocation network, which resulted in an obvious passivation zone formation at the tip of crack1. As the strain increased, the interaction between the dislocations at the crack1 tip and the γ/γ′ interface mismatched dislocation network was enhanced, and a large number of pinned dislocations formed near the crack tip (the magenta ellipse region shown in Fig. 7(e2) and (f2)). These pinned dislocations hindered the plastic deformation of the system and led to the crack1 brittle growth. Note, however, that crack2 did not have any interaction with crack1 and the γ/γ′ interface. Ultimately, the deformation work was almost entirely used for crack1 growth, which resulted in a high crack growth rate and minimized the tensile strength and plasticity of the system.

Fig. 8 shows the microstructure and dislocation evolution during the deformation of the system with two cracks distributed asymmetrically relative to the γ/γ′ interface and a distance of $d_y = 30$ Å in the *Y*-direction. Compared with the deformation system when $d_y = 0$ Å (Fig. 5), when the strain of the system was 6%, the dislocations emitted from the tip of the cracks interacted strongly with the γ/γ′ interface mismatched dislocation network, so that the interface dislocation network almost disappeared. At the same time, the dislocation entanglement zone formed at the region of the right-hand upper corner of crack1 and the left-hand lower corner of crack2 (Fig. 8(b2)), because of the interaction between crack1 and crack2. The dislocation interaction further led to the microstructure passivation of this zone, and then crack1 and crack2 merged to form a long crack (Fig. 8(c1)–(f1)). Hence, the tensile strength and plasticity of this system was weaker than the system when $d_y = 0$ Å.

4.2 Dislocation analysis

Fig. 9 shows that the dislocation density *versus* strain of the deformation system with different distances, (a) and (b) is the variation curve for the total dislocation density and proportion of pinned dislocation, respectively. During deformation, the dislocation density of the system first rapidly increased to its maximum value, then gradually decreased, and finally remained almost unchanged. Based on this analysis, we found that the significantly growth process of dislocation density corresponded to stages (I) and (II) of crack growth (*i.e.*, the crack growth incubation stage and rapid crack growth stage). The interaction between the dislocations that emitted from the crack tip and the γ/γ′ interface mismatched dislocation network was significant. After the crack growth entered stage (III) (crack

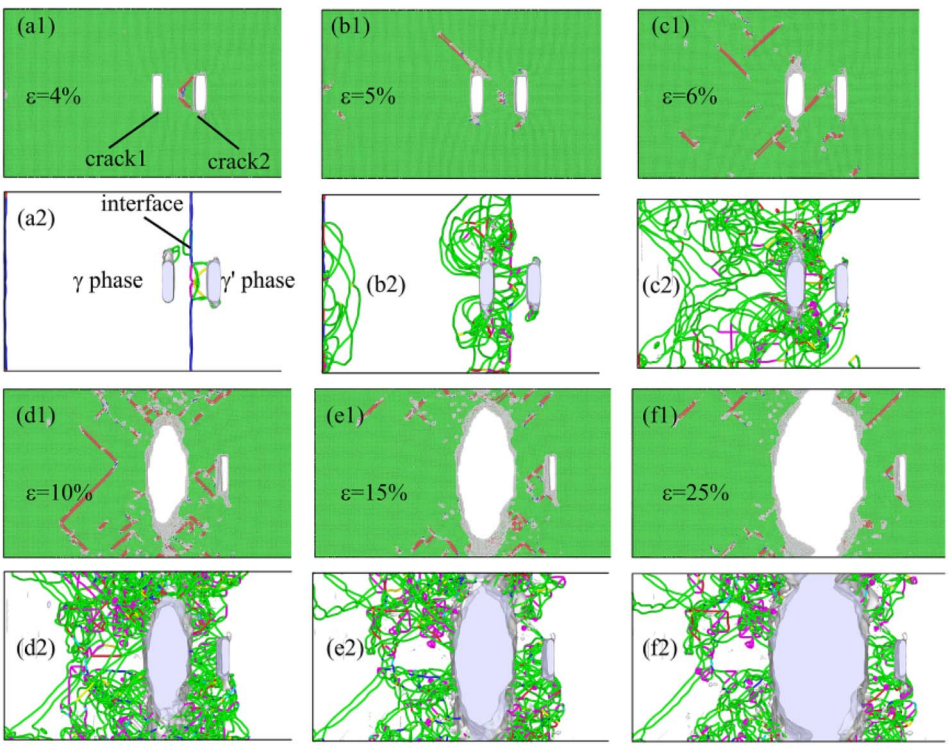

Fig. 6 The evolution of microstructure and dislocation of the tensile model when $d_x = 60$ Å, (a1–f1) the microstructure evolution of the tensile system at different tensile strain, (a2–f2) the dislocation configuration evolution of the tensile system at different tensile strain.

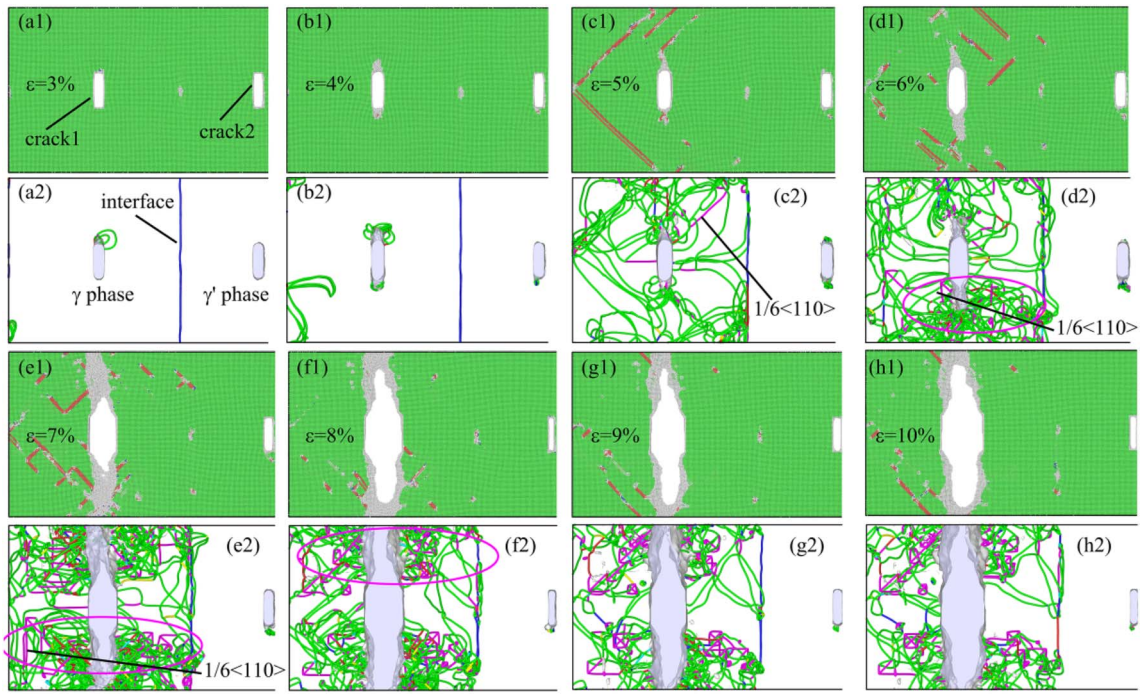

Fig. 7 The evolution of microstructure and dislocation of the tensile model when $d_x = 240$ Å, (a1–h1) the microstructure evolution of the tensile system at different tensile strain, (a2–h2) the dislocation configuration evolution of the tensile system at different tensile strain.

growth stable stage), the dislocation density gradually decreased because of the formation of a fracture surface within the system caused by crack growth. The dislocations were annihilated after they moved to the fracture surface. We compared the dislocation density *versus* strain curves of these systems with different d_x and found that as d_x increased, the

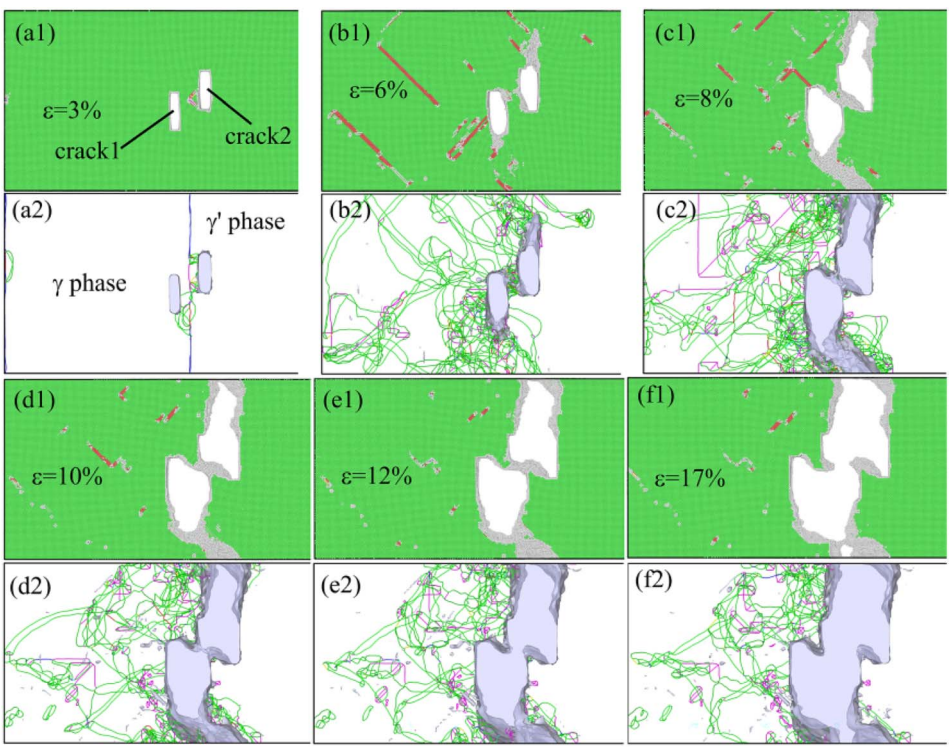

Fig. 8 The evolution of microstructure and dislocation of the tensile model when $d_x = 40$ Å and $d_y = 30$ Å, (a1–f1) the microstructure evolution of the tensile system at different tensile strain, (a2–f2) the dislocation configuration evolution of the tensile system at different tensile strain.

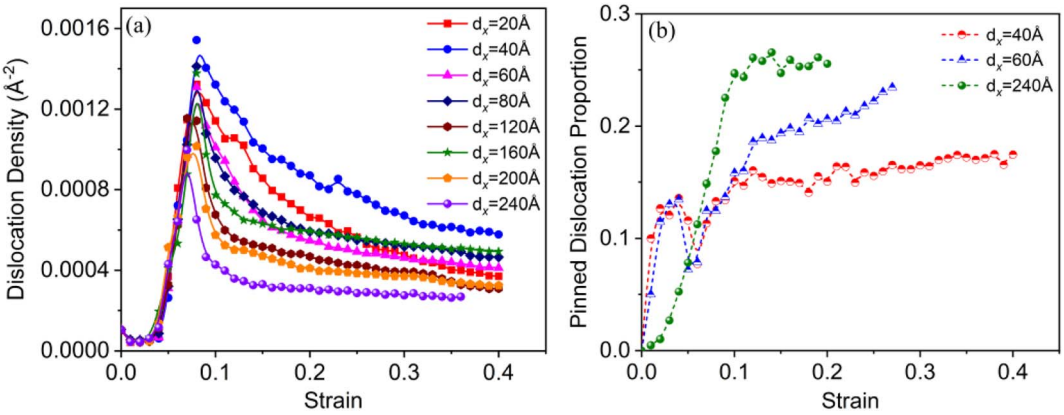

Fig. 9 Dislocation density *versus* tensile strain of the model with various crack distances: (a) the total dislocation variation, and (b) the variation of pinned dislocation proportion.

total dislocation density of the system decreased during deformation. When d_x was very small, both cracks strongly interacted with the interface mismatched dislocation network, which caused a large number of dislocations to proliferate. The proportion of pinned dislocations in the proliferated dislocations was relatively small (see the red curve in Fig. 9(b)), which increased the plastic deformation ability and tensile strength of the system. The crack slowly propagated in a plastic manner. When the d_x was large, only crack1 interacted with the interface mismatched dislocation network during the deformation, whereas crack2 hardly participated in any of the deformations, which inhibited the total dislocation density proliferation at a certain degree. The dislocation proliferation process produced a large number of immovable dislocations (accounting for about 25% of the total dislocations), which suppressed the deformation of the system. Thus, the crack propagated rapidly in a brittle manner, reducing the tensile strength and plasticity of the system.

4.3 Mechanical mechanisms

During the deformation of a metal system with cracks, a large or small plastic deformation zone (called the crack tip plastic zone) first appeared near the crack tip.[49] The shape and size of the plastic zone of the crack tip was obtained from the boundary curve equation of the crack tip:[49,50]

$$r_0 = \frac{1}{2\pi}\left(\frac{K_I}{\sigma_s}\right)^2 \quad \text{plane stress condition,} \tag{2}$$

$$r_0 = \frac{(1-2\nu)^2}{2\pi}\left(\frac{K_I}{\sigma_s}\right)^2 \quad \text{plane strain condition,} \tag{3}$$

$$K_I = \sigma\sqrt{\pi a} \tag{4}$$

where K_I is the stress intensity factor, σ_s is the yielding stress, σ is the remote stress, and a is the crack length. Because we adopted the three-dimensional periodic boundary condition in our calculation model, the deformation system was infinite in the direction of crack thickness, that is, it met the plane strain condition. Formula (3) should be used to describe the shape and size of the plastic zone at the crack tip. According to formula (3), we obtained the classical bone shape of the crack tip plastic zone in our system, as shown in Fig. 10.

Based on the relevant theories of fracture mechanics mentioned earlier, we provided the distribution maps of plastic zones at the crack tips in different crack distribution systems (d_x = 40 and 240 Å), as shown in Fig. 11(a1) and (b1), respectively. When two cracks were distributed symmetrically and the d_x was very small (d_x = 40 Å), at the beginning of the deformation, the plastic zone at the tips of crack1 and crack2 overlapped at the γ/γ′ interface (red and blue shaded areas in Fig. 11(a1)). The dislocations that emitted from the tips of crack1 and crack2 interacted strongly with the γ/γ′ interface mismatched dislocation network in the crack tip plastic zone, thereby passivating the area at the front of crack1 and crack2. In addition, the dislocations that emitted from the cracks slipped toward the γ/γ′ interface in the core region, which interacted with the γ/γ′ interface mismatched dislocation network and caused passivation in the area between crack1 and crack2 (the magenta elliptical area in Fig. 11(a1)). Because of the overlapping mechanism of the plastic zone at the crack tip, crack1 and crack2 merged to form a wide crack in the *X*-direction. The process of crack merging consumed a large amount of external deformation work, which ultimately resulted in the system having high tensile strength and good plasticity. The crack propagated slowly in a plastic manner, as shown in Fig. 11(a2) and (a3).

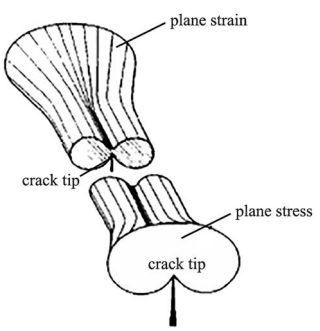

Fig. 10 Shape of crack tip plastic zone of deformation system.

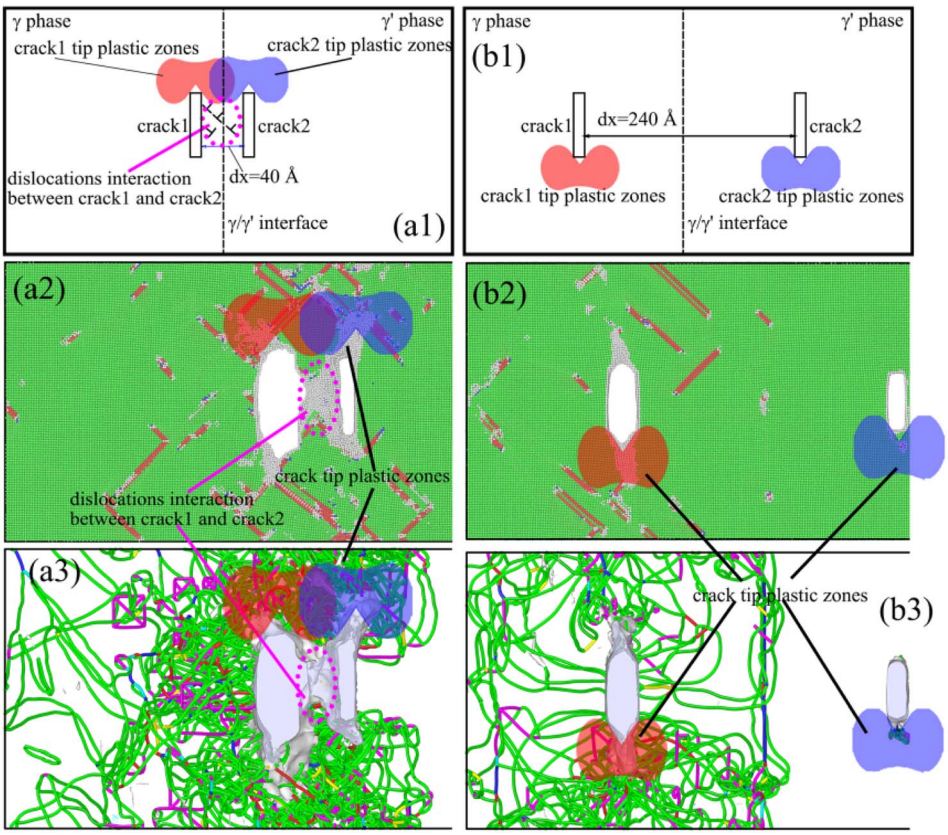

Fig. 11 Differences in the deformation and crack growth mechanism in the system with different crack distributions: (a) $d_x = 40$ Å, and (b) $d_x = 240$ Å.

For a system with two cracks distributed symmetrically and $d_x = 240$ Å, because both cracks were far away from the γ/γ′ interface, there was no overlap between the plastic zones of two cracks during deformation. Only the dislocation that emitted from the crack1 tip interacted with the γ/γ′ interface mismatched dislocation network. A large number of pinned dislocations in the γ phase hindered the plastic deformation of the system. While crack2 hardly participated in the deformation behavior of the system, almost all of the applied deformation work was used for the crack1 growth, and the system had low tensile strength and plasticity.

5. Conclusion

In this study, we used the MD method to conduct a comprehensive analysis of the Ni/Ni_3Al superalloy system, focusing on the impact of different crack distributions on deformation and crack growth behaviors. Our findings revealed that an increase in the distance between two cracks led to a significant decrease in the tensile strength and plasticity of the system. Concurrently, the crack growth rate within the system experienced a notable increase. According to the underlying mechanism, when the distance between two cracks was small, the plastic zones at their tips overlapped during deformation. This overlap resulted in strong crack interactions, which could be attributed to the interaction between dislocations that emitted from the crack tip or core with the γ/γ′ interface mismatched dislocation network. This interaction caused significant passivation in the front and middle regions of the crack tips, ultimately leading to the merging of the two cracks in the *X*-direction to form a wider crack. The emergence of two cracks consumed a considerable amount of external deformation work, resulting in the highest tensile strength and plasticity of the system.

Our study offered a potential approach to simultaneously enhance the strength as well as plasticity of multidefect systems, such as those containing internal voids and cracks. Furthermore, we provided a theoretical framework for explaining the deformation and crack growth mechanisms of systems with multiple defects. For example, by understanding and manipulating crack distributions, it may be possible to design materials with superior mechanical properties that can withstand harsh environments and loading conditions.

Data availability

All relevant data are within the paper.

Author contributions

Xinmao Qin: writing original manuscript, Wanjun Yan: computational method and analysis, Yilong Liang: review and editing manuscript, Fei Li: visualization.

Conflicts of interest

The authors declare no conflict of interest.

Acknowledgements

This work was finally funded by the Engineering Technology Research Center (No. [2019]5303), the Central Government Guides Local Science and Technology Development (No. [2019] 4011) and the Project of the Education Department of Guizhou Province (No. [2021]315).

References

1 T. M. Pollock and S. Tin, Nickel-Based Superalloys for Advanced Turbine Engines: Chemistry, Microstructure and Properties, *J. Propul. Power*, 2006, **22**(2), 361–374.
2 A. Chamanfar, L. Sarrat, M. Jahazi, M. Asadi, A. Weck and A. K. Koul, Microstructural characteristics of forged and heat treated Inconel-718 disks, *Mater. Des.*, 2013, **52**, 791–800.
3 D. McAllister, D. Lv, B. Peterson, H. Deutchman, Y. Wang and M. J. Mills, Lower temperature deformation mechanisms in a γ″-strengthened Ni-base superalloy, *Scr. Mater.*, 2016, **115**, 108–112.
4 M. Karimi, T. Roarty and T. Kaplan, Molecular dynamics simulations of crack propagation in Ni with defects, *Modell. Simul. Mater. Sci. Eng.*, 2006, **14**(8), 1409–1420.
5 W.-P. Wu and Z.-Z. Yao, Molecular dynamics simulation of stress distribution and microstructure evolution ahead of a growing crack in single crystal nickel, *Theor. Appl. Fract. Mech.*, 2012, **62**, 67–75.
6 J. Zhang and S. Ghosh, Molecular dynamics based study and characterization of deformation mechanisms near a crack in a crystalline material, *J. Mech. Phys. Solids*, 2013, **61**(8), 1670–1690.
7 P.-H. Sung and T.-C. Chen, Studies of crack growth and propagation of single-crystal nickel by molecular dynamics, *Comput. Mater. Sci.*, 2015, **102**, 151–158.
8 Y. Zhang, S. Jiang, X. Zhu and Y. Zhao, A molecular dynamics study of intercrystalline crack propagation in nano-nickel bicrystal films with (0 1 0) twist boundary, *Eng. Fract. Mech.*, 2016, **168**, 147–159.
9 Y. Zhang and S. Jiang, Investigation on dislocation-based mechanisms of void growth and coalescence in single crystal and nanotwinned nickels by molecular dynamics simulation, *Philos. Mag.*, 2017, **97**(30), 2772–2794.
10 Y. Qi, W.-P. Wu, Y.-B. Chen and M.-X. Chen, Crystal orientation dependence of crack growth and stress evolution in single crystal nickel: a molecular dynamics simulation-based cohesive zone model, *RSC Adv.*, 2018, **5**(81), 65942–65948.
11 X. Qin, Y. Liang, J. Gu and G. Peng, The Effect of Interatomic Potentials on the Nature of Nanohole Propagation in Single-Crystal Nickel: A Molecular Dynamics Simulation Study, *Crystals*, 2023, **13**(4), 585.
12 G. P. Potirniche and M. F. Horstemeyer, On the growth of nanoscale fatigue cracks, *Philos. Mag. Lett.*, 2006, **86**(3), 185–193.
13 C. B. Cui and H. G. Beom, Molecular dynamics simulations of edge cracks in copper and aluminum single crystals, *Mater. Sci. Eng.*, 2014, **609**, 102–109.
14 S. Xu and X. Deng, Nanoscale void nucleation and growth and crack tip stress evolution ahead of a growing crack in a single crystal, *Nanotechnology*, 2008, **19**(11), 115705.
15 O. Nejadseyfi and A. Shokuhfar, Molecular Dynamics Simulation of the Effects of Crystal Orientation and Grain Boundary Misorientation Angle on the Nano-Crack Growth, *J. Comput. Theor. Nanosci.*, 2014, **11**(10), 2199–2207.
16 W. Fang, H. Xie, F. Yin, J. Li, D. F. Khan and Q. Fang, Molecular dynamics simulation of grain boundary geometry on crack propagation of bi-crystal aluminum, *Mater. Sci. Eng.*, 2016, **666**, 314–319.
17 X. R. Zhuo, J. H. Kim and H. G. Beom, Atomistic investigation of crack growth resistance in a single-crystal Al-nanoplate, *J. Mater. Res.*, 2016, **31**(9), 1185–1192.
18 X. F. Liu, J. B. Wang, L. G. Sun, Y. Y. Zhang, M. L. Tian and X. Q. He, Investigation on crack propagation in single crystal Ag with temperature dependence, *J. Mater. Res.*, 2015, **30**(22), 3553–3563.
19 P. A. Gordon, T. Neeraj, M. J. Luton and D. Farkas, Crack-Tip Deformation Mechanisms in α-Fe and Binary Fe Alloys: An Atomistic Study on Single Crystals, *Metall. Mater. Trans. A*, 2007, **38**(13), 2191–2202.
20 G. Sainath and B. K. Choudhary, Atomistic simulations on ductile-brittle transition in ⟨111⟩ BCC Fe nanowires, *J. Appl. Phys.*, 2017, **122**(9), 095101.
21 S. K. Paul, S. Kumar and S. Tarafder, Orientation-dependent crack-tip blunting and crack propagation in a single crystal BCC iron, *Bull. Mater. Sci.*, 2018, **41**(6), 148.
22 Z. Wang, X. Shi, X.-S. Yang, W. He, S.-Q. Shi and X. Ma, Atomistic simulation of martensitic transformations induced by deformation of α-Fe single crystal during the mode-I fracture, *J. Mater. Sci.*, 2020, **56**(3), 2275–2295.
23 T. Tang, S. Kim and M. F. Horstemeyer, Molecular dynamics simulations of void growth and coalescence in single crystal magnesium, *Acta Mater.*, 2010, **58**(14), 4742–4759.
24 L. Chang, T. Kitamura and C.-Y. Zhou, Atomic simulation of the orientation effects on crack tip behavior in titanium single crystal, *Theor. Appl. Fract. Mech.*, 2020, **110**, 102791.
25 J. Li, L. Dong, X. Zang, X. Zhang, W. Zhao and F. Wang, Study on micro-crack propagation behavior of single-crystal α-Ti under shear stress based on molecular dynamics, *Mater. Today Commun.*, 2020, **25**, 101622.
26 K. Yashiro, M. Naito and Y. Tomita, Molecular dynamics simulation of dislocation nucleation and motion at γ/γ' interface in Ni-based superalloy, *Int. J. Mech. Sci.*, 2002, **44**, 1845–1860.
27 T. Zhu and C.-Y. Wang, Misfit dislocation networks in the γ/γ′phase interface of a Ni-based single-crystal superalloy: Molecular dynamics simulations, *Phys. Rev. B: Condens. Matter Mater. Phys.*, 2005, **72**(1), 014111.

28 W.-P. Wu, Y.-F. Guo, Y.-S. Wang, R. Mueller and D. Gross, Molecular dynamics simulation of the structural evolution of misfit dislocation networks at γ/γ′ phase interfaces in Ni-based superalloys, *Philos. Mag.*, 2011, **91**(3), 357–372.

29 N.-L. Li, W.-P. Wu and K. Nie, Molecular dynamics study on the evolution of interfacial dislocation network and mechanical properties of Ni-based single crystal superalloys, *Phys. Lett. A*, 2018, **382**(20), 1361–1367.

30 H. Yang, L. Zhu, R. Zhang, J. Zhou and Z. Sun, Influence of high stacking-fault energy on the dissociation mechanisms of misfit dislocations at semi-coherent interfaces, *Int. J. Plast.*, 2020, **126**, 102610.

31 B. Li, C. Dong, J. Yu, Q. Zhang, H. Zhou and R. Liu, Mechanical behaviour and microstructural evolution of Ni-based single crystal alloys under shock loading, *RSC Adv.*, 2018, **8**(39), 22127–22135.

32 B. Chen and W.-P. Wu, Molecular dynamics simulations of dynamics mechanical behavior and interfacial microstructure evolution of Ni-based single crystal superalloys under shock loading, *J. Mater. Res. Technol.*, 2021, **15**, 6786–6796.

33 C. Kohler, P. Kizler and S. Schmauder, Atomistic simulation of the pinning of edge dislocations in Ni by Ni3Al precipitates, *Mater. Sci. Eng.*, 2005, **400–401**, 481–484.

34 C. Cui, X. Gong, L. Chen, W. Xu and L. Chen, Atomic-scale investigations on dislocation-precipitate interactions influenced by voids in Ni-based superalloys, *Int. J. Mech. Sci.*, 2022, **216**, 106945.

35 Z.-G. Liu, C.-Y. Wang and T. Yu, Influence of Re on the propagation of a Ni/Ni3Al interface crack by molecular dynamics simulation, *Modell. Simul. Mater. Sci. Eng.*, 2013, **21**(4), 045009.

36 L. Ma, S. Xiao, H. Deng and W. Hu, Tensile mechanical properties of Ni-based superalloy of nanophases using molecular dynamics simulation, *Phys. Status Solidi B*, 2016, **253**(4), 726–732.

37 J. Yu, Q. Zhang, R. Liu, Z. Yue, M. Tang and X. Li, Molecular dynamics simulation of crack propagation behaviors at the Ni/Ni3Al grain boundary, *RSC Adv.*, 2014, **4**(62), 32749.

38 L. Ben, Z. Shiming, F. A. Essa, D. Chao, Y. Jingui and Z. Qiaoxin, Crack Propagation and Microstructural Evolution of Ni-based Single Crystal Alloy Under Shear Loads, *Rare Met. Mater. Eng.*, 2018, **47**(5), 1370–1376.

39 X. Qin, Y. Liang and J. Gu, Effects of Stress State, Crack—γ/γ′ Phase Interface Relative Locations and Orientations on the Deformation and Crack Propagation Behaviors of the Ni-Based Superalloy—A Molecular Dynamics Study, *Crystals*, 2023, **13**(10), 1446.

40 A. P. Thompson, H. M. Aktulga, R. Berger, D. S. Bolintineanu, W. M. Brown, P. S. Crozier, P. J. in 't Veld, A. Kohlmeyer, S. G. Moore, T. D. Nguyen, R. Shan, M. J. Stevens, J. Tranchida, C. Trott and S. J. Plimpton, LAMMPS - a flexible simulation tool for particle-based materials modeling at the atomic, meso, and continuum scales, *Comput. Phys. Commun.*, 2022, **271**, 108171.

41 L. Ma, S. Xiao, H. Deng and W. Hu, Atomic simulation of fatigue crack propagation in Ni3Al, *Appl. Phys. A*, 2014, **118**(4), 1399–1406.

42 Y. Zhang, S. Jiang, X. Zhu and Y. Zhao, Mechanisms of crack propagation in nanoscale single crystal, bicrystal and tricrystal nickels based on molecular dynamics simulation, *Results Phys.*, 2017, **7**, 1722–1733.

43 G. P. Purja Pun and Y. Mishin, Development of an interatomic potential for the Ni-Al system, *Philos. Mag.*, 2009, **89**(34–36), 3245–3267.

44 B. Chen, W.-P. Wu and M.-X. Chen, Orientation-Dependent Morphology and Evolution of Interfacial Dislocation Networks in Ni-Based Single-Crystal Superalloys: A Molecular Dynamics Simulation, *Acta Mech. Solida Sin.*, 2020, **34**(1), 79–90.

45 J. D. Honeycutt and H. C. Andersen, Molecular dynamics study of melting and freezing of small Lennard-Jones clusters, *J. Phys. Chem.*, 1987, **91**(19), 4950–4963.

46 D. Faken and H. Jónsson, Systematic analysis of local atomic structure combined with 3D computer graphics, *Comput. Mater. Sci.*, 1994, **2**(2), 279–286.

47 A. Stukowski, Visualization and analysis of atomistic simulation data with OVITO–the Open Visualization Tool, *Modell. Simul. Mater. Sci. Eng.*, 2010, **18**(1), 015012.

48 A. Stukowski, V. V. Bulatov and A. Arsenlis, Automated identification and indexing of dislocations in crystal interfaces, *Modell. Simul. Mater. Sci. Eng.*, 2012, **20**(8), 085007.

49 P. Lopez-Crespo, D. Camas, F. V. Antunes and J. R. Yates, A study of the evolution of crack tip plasticity along a crack front, *Theor. Appl. Fract. Mech.*, 2018, **98**, 59–66.

50 J. M. Vasco-Olmo, M. N. James, C. J. Christopher, E. A. Patterson and F. A. Díaz, Assessment of crack tip plastic zone size and shape and its influence on crack tip shielding, *Fatigue Fract. Eng. Mater. Struct.*, 2016, **39**(8), 969–981.